Energy 249 (2022) 123515

Contents lists available at ScienceDirect

Energy

journal homepage: www.elsevier.com/locate/energy

Effects of iron on coal pyrolysis-derived soot formation

Dun Li, Jianmin Gao*, Ziqi Zhao, Qian Du, Heming Dong, Zhaoyang Cui

School of Energy Science and Engineering, Harbin Institute of Technology, Harbin, 150001, China

ARTICLE INFO

Article history:
Received 24 May 2021
Received in revised form
12 February 2022
Accepted 16 February 2022
Available online 28 February 2022

Keywords:
Soot
Coal
Iron
Microstructure
Chemical structure

ABSTRACT

Soot formation is one major challenge in developing clean and efficient utilizes based on hydrocarbon fuels. In this work, ferric nitrate was selected as an iron additive to be loaded into pulverized coal, and the pyrolysis experiment with an inert atmosphere was conducted in a high-temperature drop tube furnace (DTF). The physical and chemical character of the soot obtained from coal samples with different iron content were analyzed to explore the effect of the soot format process. The results showed that the soot yield was reduced 7% and 23%, respectively, at the same conditions when the content of iron in the coal sample was 0.51% and 0.87%. After iron was added, the diameter of soot primary particles was reduced from 50.8 nm to 37.4 and 37.8 nm, and the D_f of soot aggregates increased, indicating that iron inhibited the growth process of soot primary particles and promoted the agglomeration between particles. Thus, the degree of graphitization of soot increased. In addition, the content of C—O functional groups in soot derived from coal with iron addition increased significantly, which implied that the participation of iron enhanced the oxidation reaction of soot.

© 2022 Published by Elsevier Ltd.

1. Introduction

As a traditional fossil fuel, coal currently supplies 37% of global electricity, and it will still play a vital role in the next two decades, especially in developing countries [1]. Coal is also widely used in metallurgical processes, gasification, and heating supply and as a raw material for many industrial chemicals [2]. Soot particles generated during coal utilization are significant contributors to fine particulate matter in the atmosphere. Soot has dire consequences on human health [3–5], leads to haze, and causes the greenhouse effect [6,7]. Therefore, comprehensively understanding the mechanisms of coal pyrolysis and combustion of soot formation to search for possible solutions to decreasing the production of soot.

The formation process of soot is divided into five processes including: nucleation, surface growth, coagulation, aggregation and oxidation. The final soot production is a process where formation and oxidation compete with each other. Soot formation of simple hydrocarbon combustion and internal combustion engines has received extensive attention [8–16]; however, the understanding of soot formation is incomplete, especially during the combustion of solid fuel. Coal pyrolysis is the first step in coal gasification and combustion [17]. Devolatilization is the first step during the thermal conversion of solid carbon fuels such as coal and biomass, which is different from simple hydrocarbon fuels. The primary pyrolysis process of coal will release gaseous volatiles, small molecular hydrocarbons and tar containing rich PAHs. Tar and volatiles are important precursors of soot during coal second pyrolysis [18–21]. Polymerization and cracking of PAHs in tar compete with each other at high temperatures. Therefore, soot derived from coal pyrolysis involves not only the growth of aromatics and small free radicals through the Hydrogen-abstraction-acetylene-addition (HACA) [22,23]and clustering of hydrocarbons by radical-chain reactions(CHRCR) [24,25] mechanism, but also the breaking and reformation of rings [26]. In addition, the macromolecular PAHs in tar can directly polymerize and grow on the surface of soot particles, which complicates the entire soot generation.

The process of soot formation during coal pyrolysis is affected by many factors, including coal type, pyrolysis conditions (temperature, time and atmosphere), and inorganic metal content. The experimental results of Nenniger et al. [27], Wornat et al. [28] and Zeng et al. [29] showed that the increase in temperature and residence time in inert atmosphere and enhance the conversion of tar to soot, while the sum of the tar and soot remains constant. Ma et al. [30,31]found that soot obtained from coal pyrolysis in the flue gas environment generated by $CH_4/H_2/N_2/O_2$ is significantly lower than that under inert atmosphere, and the oxygen-containing components (OH, O) in environment inhibited the soot formation. Chang et al. [18,32] [][]investigated the effects of CO_2 on the

* Corresponding author.
E-mail address: yagjm@hit.edu.cn (J. Gao).

https://doi.org/10.1016/j.energy.2022.123515
0360-5442/© 2022 Published by Elsevier Ltd.

characteristics of soot during coal pyrolysis. The results show that CO_2 in pyrolysis environment can enhance the soot formation and advances the dehydrogenation, while the degree of graphitization of soot increases and the reaction activity decreases. Coal is rich in inorganic metal salts which will participate in soot formation and oxidation in coal thermal conversion. Researchers have considerably investigated the effect of alkali/alkaline earth metal species (AAEMs) on solid fuel soot [33–36], but few studies related to transition metals have been conducted. The mechanism of iron, as a common transition metal, on the growth and oxidation of soot during simple hydrocarbon combustion and internal combustion engine operation has attracted considerable attention. The effect of iron participation on the amount of soot generation has been discussed [37]. Iron additives have been shown to promote soot formation under some conditions [38]. Studies have shown that the addition of iron pentacarbonyl [39], and ferrocene [40] increases soot volume fractions in premixed flames. The iron can be integrated with the soot through an early condensation, and the induced nucleation can override "homogeneous" nucleation via PAHs and free radicals format and growth when concentration is sufficiently high [41]. Howard and Kausch [42] proposed that metal additives can also affect soot formation with the enhancement in soot oxidation and burnout mechanisms. Kim et al. [43] found through the study of soot oxidation kinetics that the pentacarbonyl iron in the flame reduces the oxidation activity of soot and enhances the soot burnout. Steffen et al. [44,45] comprehensively studied the oxidation process of soot with Fe_2O_3 catalyst. They found that oxygen from the gas phase to the soot via the Fe_2O_3 mainly occurs by physical contact points of soot and catalyst, and lattice oxygen of Fe_2O_3 also is mainly involved in the soot oxidation. Kim et al. [46,47] quantitatively analyzed the existence form of iron in the isooctane added iron pentacarbonyl diffusion flame and the soot production using in situ methods. The experimental results showed that the iron atoms formed by carbonyl iron play an important role in the soot formation process The direct catalytic reaction of Fe is the main reason for the reduction in soot. Braun et al. [48] found that adding ferrocene to diesel fuel is conducive to the formation of aliphatic structure. This formation leads to changes in the nanostructure of soot. Ultimately, soot has better oxidation activity. However, the effects of Fe on soot derived from coal are still largely unclear due to the inherent complexity of tars, and few related studies are available.

The research on soot production during coal pyrolysis is still insufficient, especially the effect of metals on soot formation during coal pyrolysis. Different from fuels such as methane, ethylene, and diesel, coal soot is derived from the second reaction process of coal tar. Coal tar is abundant in polycyclic aromatic compounds, essential precursors of soot. At present, the mechanism regarding the influence of metals, especially iron, on the conversion process of coal tar to carbon soot is not clear. Various ions, radicals, and gases are also produced during coal pyrolysis. The effect of these substances on carbon soot production with the involvement of iron needs further investigation. This paper analyzes the changes in the physicochemical properties of carbon soot generated by coal pyrolysis with and without the participation of iron and aims to obtain the mechanism of iron influence on soot derived from coal pyrolysis. Hoping to provide theoretical support for the feasibility of adding metals to coal to reduce soot emissions through laboratory experiments. In this work, $Fe(NO_3)_3$ as the additive was doped in pulverized coal, and its influence in process of coal pyrolysis was investigated. Transmission electron microscopy (TEM), and Raman spectrum were conducted to obtain the microstructure information of soot particles. FTIR and XPS were performed to reveal the information of chemical functional groups in soot particles.

2. Experiment

2.1. Experiment system

This work used a drop tube furnace (DTF) shown in Fig. 1, which could provide a stable high pyrolysis temperature field. The center of DTF is a corundum tube with a diameter of 80 mm and a height of 1800 mm. The heating area divided into four parts for heating, and equipped with corresponding thermocouples for temperature detection. During the experiment, the temperature was stable at 1250 °C. Before the pyrolysis experiment, 9L/min of N_2 was introduced into the furnace through a porous gas distributor to exhaust the air. Pulverized coal sample was supplied at a speed of 0.1 g/min by the controllable micro-feeder and carried by 1L/min of N_2 into heating area. The pyrolysis gas was obtained through a sampling gun. The particles larger than 10 μm in diameter are removed by a cyclone, and then enter the ELPI and volume sampler for subsequent analysis. Before the pyrolysis gas enters the volume sampler, it is diluted with 8L/min N_2. There is a flow controller behind the volume sampler and adjusted to 18L/min before sampling, and the sampling ends when the value drops to 17L/min. More details of this experimental system are described in our previous work [49,50].

2.2. Experiment samples

Yimin lignite (YM) was selected as the experimental coal sample and was ground into a diameter of 38–125 μm. Metal elements in YM coal were removed through HCl washing to eliminate the influence of other metal elements on the experimental results. The results of proximate analysis and ultimate analysis of YM and YMH are presented in Table 1. The content of major non-metallic elements (C, H, N, and S) in the coal sample did not change significantly after acid-washed. The coal sample after the removal of metal elements is denoted as YMH, and our previous work show that acid-washed has no significant effect on non-metallic elements in coal [51]. $Fe(NO_3)_3 \cdot 9H_2O$ was selected as the iron additive and loaded onto the YMH by the impregnation method. YMH sample loaded with iron was named YMH-Fe. Metal elemental contents in the YM, YMH, and YMH-Fe coal samples are shown in Table 2, obtained through an atomic emission spectrometer (ICP-AES). The content of metal elements in YMH is much lower than YM, indicating that the acid-washed process removes metal elements effectively. The iron content in YMH-Fe1 and YMH-Fe2 is 0.51% and 0.87%, respectively. The content of Na, Ca, Mg, and Al in

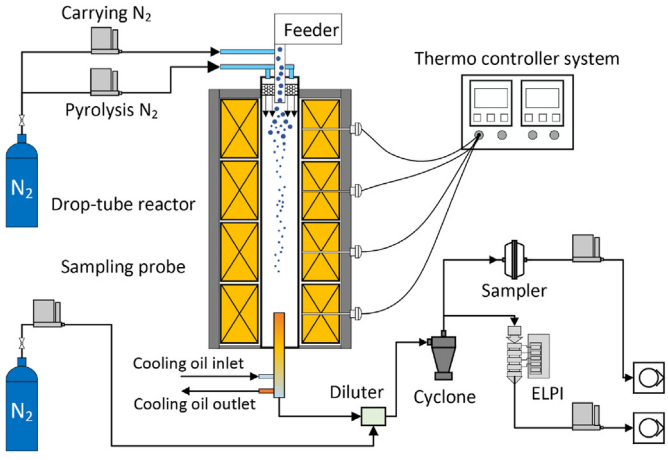

Fig. 1. Schematic of the experimental system.

Table 1
Properties and ultimate analysis of YM and YMH coal samples.

	Proximate analysis (wt. %, d[a])			Ultimate analysis (wt. %, d[a])			
	V_d	FC_d	A_d	C_d	H_d	N_d	S_d
YM	42.30	41.19	16.51	68.48	4.11	0.99	0.19
YMH	42.70	44.84	12.46	67.89	4.26	0.96	0.18

[a] Calculated by difference; d, dry basis; V, volatiles; Fc, Fixed Carbon; A, Ash.

Table 2
Main metal element contents in coal samples.

	Na	K	Ca	Mg	Fe
YM	0.0534	0.0294	0.7947	0.0832	0.7947
YMH	0.0108	0.0241	0.1082	0.0083	0.1082
YMH-Fe1	0.0071	0.0399	0.0529	0.0110	0.5109
YMH-Fe2	0.0048	0.0423	0.1057	0.0109	0.8749

unit: wt.%, d; d, dry basis.

acid-washed coal with different Fe content was low and similar. Therefore, it is concluded that changes in physicochemical properties of coal-derived soot are caused by different content of Fe (see Table 2).

2.3. Analytical techniques

Before the analyses of soot particles with TEM, the soot was dissolved in ethyl alcohol with the assistance of ultrasound for 20 min. The bright field images were obtained at 20 000 × and 400 000 × magnification through an electron microscope (JEOL-2100F) operating at. 200 kV. Raman spectra of three coal soot were acquired from Raman spectrometer (LabRAM HR800 Horiba) with a He/Ne solid-state diode laser excitation source (532 nm). An objective lens with 100 × magnification was used. Each sample were measured on three different areas and spectral were collected via a thermoelectric cooled CCD camera. Accumulatively scan 10 times for per test and the exposure time was adjusted to 8s for each scan.

FTIR of soot was obtained with a Nicolet 5700 spectrometer in the range of 4000–400 cm^{-1}. Soot collected from filter was prepared into KBr pellets of uniform size at a ratio of 1:1000 to facilitate semi-quantitative analysis. Two KBr pellets were made for each soot to increase the reliability of the results. Chemical state of element at the surface of soot was obtained from XPS (ESCALAB 250Xi). C1s and O1s peaks were recorded at 20 eV pass energy and all spectra were calibrated to reproduce the C1s peak of contaminant carbon (BE = 284.6 eV).

3. Result and discussion

3.1. Yield of soot

Dichloromethane extraction was used to separate soot and tar from particles collected on glass fiber membrane, and the specific operation procedure could refer to our previous work [49–51]. Different tar and soot yield information are shown in Fig. 2 (a). The sum of soot and tar yields in the pyrolysis products were negatively correlated with the Fe content in the coal samples. Compared with YMH, the tar yield of YMH-Fe1 was reduced, while the soot yield did not change significantly. In contrast, the tar yields of YMH-Fe1 and YMH-Fe2 were similar, but the soot yield of the latter was significantly lower than that of the former. This result indicates that the effect of iron on soot formation is complex and related to iron concentration in coal. The soot yield of YMH-Fe2 showed a reduction of approximately 19% in the amount of soot when compared with the YMH. The above results indicate that the addition of iron during coal pyrolysis catalyzes the cracking of tar and inhibits the final production of soot. Natalia et al. [52], Ma et al. [53], and Zhang et al. [54] investigated the effect of an iron-based compound on exhaust emissions from diesel and found that the particles emission was drastically reduced. In Natalia's experiment, the amount of soot collected in filters decreases around 50% when iron content in fuel is 0.15%. Compared with the diesel engine, the iron added in this experiment did not reach high efficiency in reducing soot. As a soot precursor, coal tar is rich in PAHs, which are more easily converted to soot than aliphatic hydrocarbon fuels (diesel, etc.). During coal pyrolysis, the contact tightness of coal tar with added iron is lower than that of fuel oil with iron blending. Our previous study reduced the carbon soot yield by 48% when the iron addition in this paper reached 3% in the YMH sample. Compared with the experiments related to the diesel engine, the experiments were carried out in an inert atmosphere without oxygen. Despite iron promoting the soot oxidation reaction, the available oxidant during coal pyrolysis is limited. The number of concentration particles in pyrolysis gas distribution of different coal samples is shown in Fig. 2 (b). The distribution curves of the three samples are similar, and 99% of the particles are smaller than 0.5 μm in diameter (Stokes diameter). After ferric nitrate is added, the peak near 0.12 μm decreases gradually as the iron content in the coal sample increases. Therefore the participation of iron affects the early aggregation process of primary particles. The mass concentration of the pyrolysis particles of the three kinds of coal samples and the particle size distribution all have a peak around 0.12 μm and similar distribution rules. In this section, the mass fraction of submicrometer particles (the first seven stages of ELPI) was calculated, and the results of YMH soot were 5.6%, significantly higher than YMH-Fe1 (1.1%), and YMH-Fe1 (1.5%), respectively.

3.2. Microstructure of soot obtained from TEM

The morphology of soot of three kinds of coals was observed by TEM. Fig. 3 shows that soot particles are irregular fractal aggregates and composed of tens to hundreds of primary carbon particles. The aggregation of primary particles in YMH-Fe2 soot is more tightly than the other two soot. The diameter of primary particles in soot was counted by ImageJ (an image processing software), and fractal dimension D_f of the soot aggregate was calculated in combination with the method described in the literature [55–57], shown in Fig. 4 (a) and (b). The average primary diameter of YMH soot is 51.1 nm and is mainly concentrated in the range of 26–50 nm, which is larger than the soot produced during the combustion of simple hydrocarbon fuels [57–60]. This result indicates that the materials produced during the first pyrolysis of coal are more easily converted into soot. The average primary particle diameter of YMH-Fe1 and YMH-Fe2 soot samples are 38.7 and 39.1 nm, respectively, approximately 24% lower than that of YMH soot. Also, the particle size distribution range of the primary particles of YMF-Fe1 and YMF-Fe2 soot is reduced, i.e., the uniformity of the primary particles is improved. The Natalia et al. [52] experiment found that all soot primary particle diameters were similar (36 nm–39 nm) independent of the iron content. However, Zhang [54] shows that the primary particle diameters of soot decrease with the iron content in fuel. Particle oxidation may occur at each stage in the process of soot formation, and the eventual size of primary particles of soot depends largely on balance between the soot formation and burnout processes. Surface growth refers to the process in which gaseous species attach to the surface of pre-existing soot and the incorporation of the particle phase. The importance of PAH addition on particle surface in soot mass growth has been demonstrated.

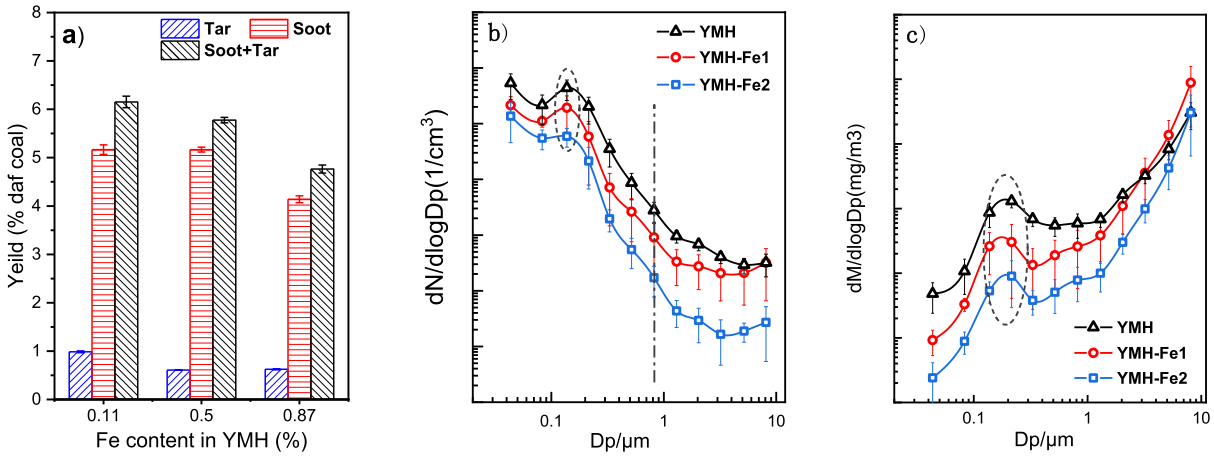

Fig. 2. a) Yields of soot, tar, and soot + tar, b) the number concentration distribution, the mass concentration of the soot derived from different coal.

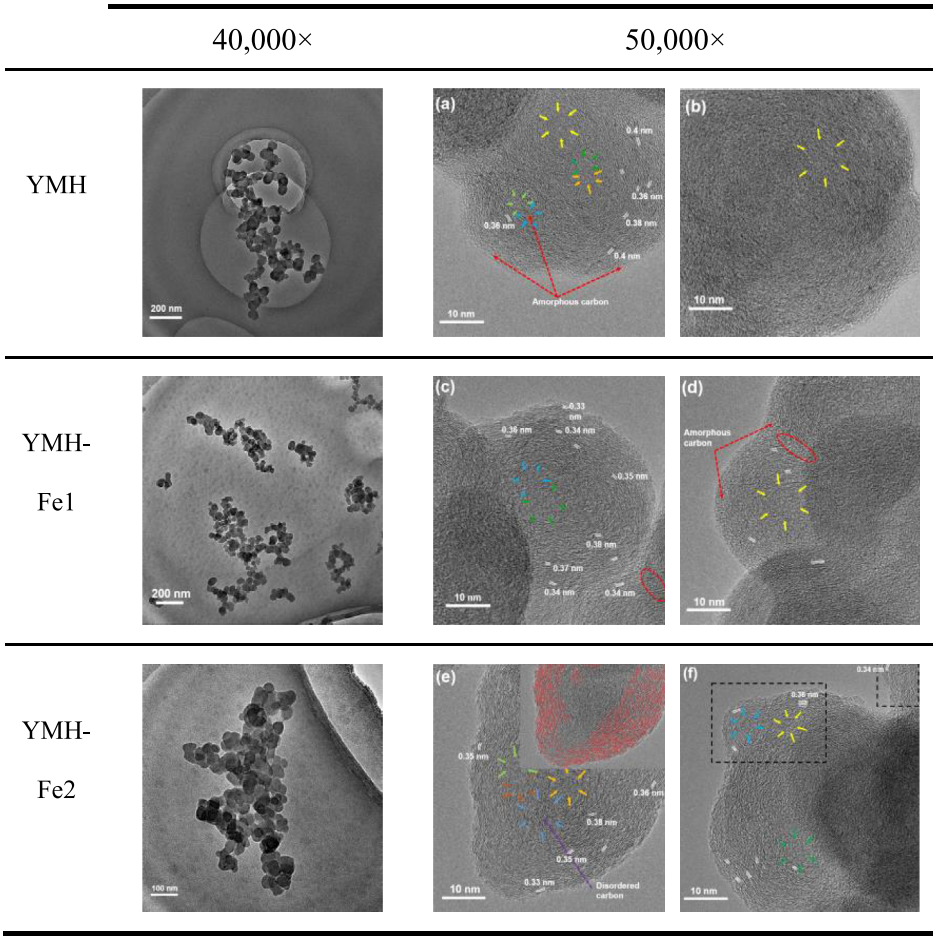

Fig. 3. Representative TEM images of all soot samples. (The area surrounded by arrows is the nucleus of soot particles; The short white line illustrates the crystallite layer; The upper right of (e) is a schematic diagram of the microcrystalline structure extraction.

The particle size analysis results show that the involvement of iron inhibits the accumulation process of PAH on the particle surface. In addition, the number of irregular primary particles in the soot aggregate increases, Simonsson et al. [38] also observed similar phenomena in their experiments. The involvement of iron has a facilitating effect on the soot oxidation reaction, which is one of the reasons for the decrease in particle size. The D_f of the three types of soot is between 1.86 and 2.04, similar to the results of previous research [57]. The D_f of YMH-Fe2 soot is larger than those of YMH and YMH-Fe1 soot, which means the primary particles in the soot are agglomerated more tightly, and fewer aggregate branches are formed, which is consistent with the results observed in Fig. 3. The participation of iron in the soot generation process of coal pyrolysis will increase the collision and agglomeration between primary

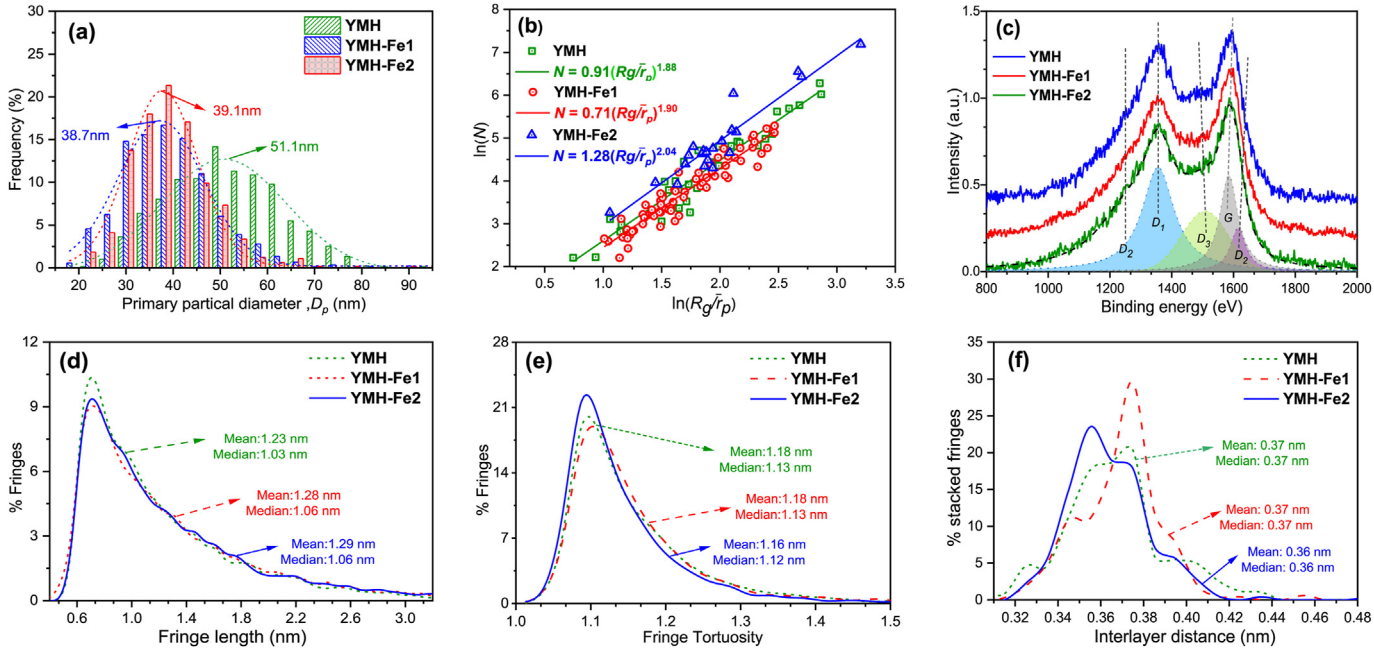

Fig. 4. (a) Primary particle diameter distribution; (b) D_f of soot aggregation; (c) Raman spectrum of soot; (d)–(f) Fringe length, tortuosity and interlayer distance of soot.

particles.

Fig. 3. (a) (f) shows the HRTEM of the three soot samples and related information about microstructure. The primary particles of the three soot samples have similar structures, and all show an "onion-like" core-shell structure. Among all soot samples, the core of the primary particle is formed by the collision and condensation of multiple nascent nanoparticles. This observation indicates that PAHs produced in the primary pyrolysis of coal can quickly form nascent soot nanoparticles. Unlike simple aliphatic hydrocarbons that form the ring and aromatic free radicals, amounts of PAHs around the nascent nanoparticles will create a relatively loose and thin external carbon crystallite layer. During the collision and condensation process, these nascent nanoparticles are wrapped by more crystallite layers to form primary particles. The shell formed by the crystallite layers outside the core of YMH soot is thicker than that of YMH-Fe1 soot, but the layer stacking is more disordered. Some particles of soot were wrapped with an amorphous carbon crystallite layer, as shown in Fig. 3 (a) and (d), and these amorphous carbon layers are composed of aliphatic compounds and simple PAHs with 3–5 rings. Primary particles of YMH-Fe2 soot have more cores, and the number of stacked layers of crystallite outside the core is reduced, but the arrangement is more orderly. The above-mentioned amorphous carbon outer layer does not appear in the YMH-Fe2 soot. Structures with a higher degree of graphitization are observed at the edges of the primary particles, as shown in the black dotted frame Fig. 3 (f). These structures may be formed by the collision and condensation of mature soot and nascent nanoparticles. A series of processing on HRTEM pictures referred to the method proposed by other researchers [61,62] to facilitate the extraction of the length, curvature and spacing of crystallite layers of soot for effectively evaluating the microstructure of soot. The selection of the soot crystallite in image processing process is artificial. In order to reduce the error in the processing process, the main choice is the crystallites that are farther from the core and clearer. Fig. 4 (d) shows that the lengths of crystallite in all soot are mainly distributed between 0.4 and 3 nm. After iron is added, the average length of the crystallites in soot increases from 1.23 nm to 1.29 nm, and the peak shifts to the right. Therefore, the participation of iron promotes the growth of crystallites and the degree of graphitization of soot particles. Curvatures of crystallite in soot are mainly distributed between 1.05 and 1.25, shown in Fig. 4 (e). The median and mean values of crystallites curvature in YMH-Fe2 soot are lower than those in other soot, and the average spacing of crystallites in YMH-Fe2 soot is also smaller than those in others. The crystallites curvature of soot is mainly controlled by the number of odd rings in the aromatic plane. Surface growth is primarily the process of adhesion of PAHs to the soot surface and the incorporation of the particle phase. Thus the involvement of iron reduces the amount of odd-ring substances in coal tar. Different from other literature [46,52,63,64], iron-containing particles are not observed in the TEM of YMH-Fe soot may be due to the PAHs produced by the primary pyrolysis of coal are more likely to nucleate than iron.

3.3. Raman spectrum analysis of soot

Fig. 4 (c) presents the Raman spectra of the soot sample derived from three kinds of coal pyrolysis. The spectra for each iron content correspond to the average of three spectra, and thus, they have a certain degree of representativeness. The pyrolysis conditions of all coal samples remain the same. As shown in Fig. 4 (c), the spectra are all similar, and they all show two prominent peaks around 1355 and 1590 cm^{-1}, which correspond to the typical D and G peaks of soot, respectively. The insignificant change in the peak position illustrates that the iron does not change the basic core-shell structure of soot during formation.

Five band fitting method was used for first-order Raman spectra for quantitative spectral analysis, as shown in Fig. 4 (c). The G band around 1590 cm^{-1}, D1 band around 1355 cm-1, D2 band around 1620 cm^{-1} and D4 around 1250 cm-1 were used as Lorentzian functions. The D3 band around 1510 cm^{-1}, representing the amorphous carbon, was used as a Gaussian function. Some parameters have been demonstrated to be related to graphite-like structure and amorphous carbon in soot. In this work, full widths at half maximum of the D1 (D1 FWHM) band and *R3* ($R3 = ID3/ID3 + ID2 + IG$) were adopted to observe most chemical structure

differences in nanostructure among three kinds of soot samples. Typically, *FWHM* of D1 band represents the degree of graphitization of carbonaceous materials, *R3* can reflect the content of amorphous carbon in soot [65–67], *La* is the in-plane graphitic crystallite size of carbonaceous materials and is inversely proportional to I_{D1}/I_G, and *I* is the integrated area of each band [68]. As the iron content in the coal sample increases, the mean value of *R3* decreases, as shown in Table 3. This founding means the relative content of amorphous carbon in the soot decreases. The *D1 FWHM* value of YMH-Fe2 soot is significantly reduced. The I_{D1}/I_G ratios of soot from different coal samples show a ranking of YMF-Fe2 < YMF-Fe2 < YMF. The result illustrates the soot from coal with iron are more ordered and contains less disordered carbon. As the disordered carbon is more accessible to oxygen attack [69], and a decrease of chemical heterogeneity and an increase of structural order upon oxidation [70]. This indicates that iron is involved in the formation of soot during the coal pyrolysis, which mainly promotes the oxidation reaction of soot. *La* calculated by Raman spectroscopy increase with the rise iron content of coal sample. The results mentioned above can also be observed in Fig. 3, which shows that the iron in the coal sample promotes soot oxidation during the pyrolysis process, mainly occurring in the amorphous carbon region. In addition, the size of the formed crystallite layer is more significant with the participation of iron. These phenomena all promote the overall graphitization degree of soot particles.

3.4. Chemical characters of soot

The contents of C, H, N in soot were measured with an elements analysis instrument (VARIO Macro cube). As shown in Fig. 5 (a), the C in soot decreases as the iron content in coal increases from 0.11% to 0.87%. The C/H ratios of YMH-Fe1 soot and YMH-Fe2 soot are higher than that of YMH, which means that dehydrogenation during the soot formation process is enhanced. This result is also consistent with the phenomenon that iron increases the degree of graphitization of soot produced from coal pyrolysis. Fig. 5 (a) also shows that the iron content in soot is positively correlated with the iron content in the corresponding coal sample. The migration rate of iron in coal to soot was calculated. After ferric nitrate is added, the iron content in the soot increases. However, the migration rate of iron from the coal sample decreases from 8% to 2%, indicating that ferric nitrate did not directly participate in the formation of soot and indirectly affected the soot formation by changing the formation of coal primary pyrolysis products and their secondary reactions. That may be the reason for iron-containing soot samples were not being observed in TEM.

Fig. 5 (b) presents the infrared absorption spectra of soot. As marked in the spectra, the stretching vibration of aliphatic C–H is generally a group of bands in the 3000-2800 cm^{-1} region, and that comes mainly from methyl, methylene groups, or saturated rings linked to aromatic rings on PAHs or methylene bridges to connect different PAHs. The peaks at 1380 cm^{-1} and in the 1450 cm^{-1} spectrum which is attributed to the in-plane deformation of aliphatic C–H bonds, confirm the presence of aliphatic groups [71]. The content of aliphatic groups of YMH-Fe1 soot is significantly higher than those of YMH and YMH-Fe2 soot. K. O. Johansson [25] suggested that RSR (resonance stabilized radical) on soot surfaces could provide sites for the chemisorption of small hydrocarbons. Thus the surfaces of soot particles may have more aliphatic character than the rest of the graphitic shell. Iron during pyrolysis may promote the cracking of these aliphatic chains, inhibit the surface accumulation process of PAHs, and reduce carbon soot production. However, this reaction requires a certain concentration of iron in the coal sample. Therefore, different iron concentrations will have various effects. In the 1000-1800 cm^{-1} region lie the stretching bands of C–O groups in alcohols or phenols and ethers (1080-1240 cm^{-1}), that of C=C groups in aromatics (1580-1590 cm^{-1}), and that of C=O groups (1650-1720 cm^{-1}) are observed; they are typically present in carboxylic acids, ketones, aldehydes, esters, and lactones [57,72,73]. The IR spectra of YMH-Fe1 and YMH-Fe2 soot contain more significant absorption peaks of C–O groups, and the peaks of aromatic C=C vibration are more obvious. This trend indicates that iron addition affects the formation of oxygen-containing functional groups on the soot surface in coal pyrolysis, especially C–O groups. The 925-700 cm^{-1} region belongs to the bending vibration of aromatic out-of-plane hydrogens (OPLA). Four parameters $A_{1\text{-}4}$ were used to analyze the effect of the addition of iron on functional groups of soot. A_2 is the ratio of methyl to methylene, and the length of the aliphatic chain of soot is shorter when A_2 is higher. A_1, A_3, and A_4 were obtained by dividing the area of OPLA, C=O groups and C–O groups to the aromatic C=C band area. They represent the substitution degree of aromatic compounds and the trend of C–O and C=O content in soot. After ferric nitrate is added, the representative aromatic hydrogen abundance parameter *A1* of soot increases, as shown in Fig. 5 (c). Correspondingly, the YMH-Fe2 soot spectrum has a significant shoulder peak at 3050 cm^{-1}. The parameter *A2* of YMH soot is much larger than those of YMH-Fe1 and YMH-Fe2 soot, which indicates that the participation of iron reduces the length and number of aliphatic branches in soot. The infrared spectra of YMH-Fe1 and YMH-Fe2 soot show an obvious peak at 1380 cm^{-1}, which means that the number of methyl groups connected to the aromatic ring increase. As the iron involved in the pyrolysis process increases, the content of C–O functional groups in the soot increases.

The high-resolution scan results of the nominal C1s and O1s regions of soot are shown in Fig. 5 (d) and (e), respectively. All peaks were deconvolved to obtain more information about carbon bonding fractions and oxygenated functional groups. As shown in Fig. 5 (f), the relative content of C–O functional groups in the aliphatic group of soot decreases that in the presence of iron. Moreover, C–O functional groups on the aromatic ring increase significantly, especially in YMH-Fe2 soot. Meanwhile, the C/O ratio of YMH-Fe2 soot is also reduced considerably, which implies that the oxidation reaction increases during the soot formation. Fig. 5 (f) shows that the content of sp^2 hybrid carbon in soot gradually increases with the rise in iron content in coal. The ratio of sp^2/sp^3 also increases significantly, which implies a higher degree of graphitization of soot.

Table 3
D1 FWHM, *R3*, *La* obtained from Raman spectrum.

	D1 FWHM	R3	I_{D1}/I_G	La
YMH	133.4 ± 8.0	0.47 ± 0.03	1.87 ± 0.05	2.72 ± 0.15
YMH-Fe1	133.2 ± 1.9	0.46 ± 0.01	1.40 ± 0.06	3.12 ± 0.24
YMH-Fe2	123.7 ± 2.9	0.43 ± 0.06	1.28 ± 0.02	3.39 ± 0.15

4. Discussion

This work mainly studied the effect of iron additive on the physical and chemical characteristics of soot during coal pyrolysis. Ferric nitrate was selected as the iron source and loaded onto the surface of coal powder by dipping method, which was mainly in the form of physical contact. YMH, YMH-Fe1, YMH-Fe2 coal samples were subjected to pyrolysis experiments with the same pyrolysis conditions. Experimental analysis concluded that participation of iron effects the yield, microstructure and chemical functional groups of soot, and the effects related to the concentration of iron in the coal sample.

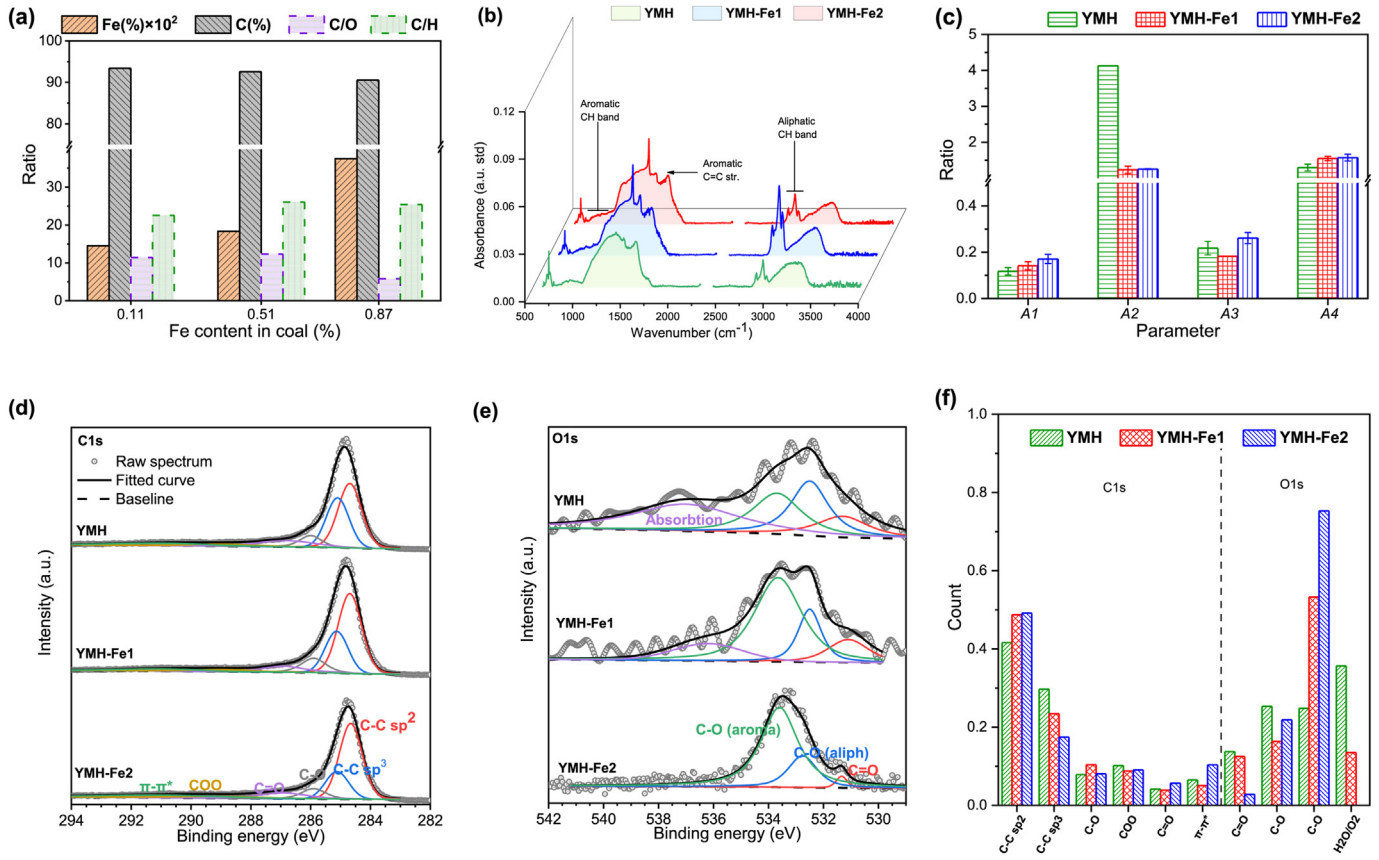

Fig. 5. (a) Content of C, H, N in soot; (b) FTIR spectrum of soot; (c) Parameter $A_{1\text{-}4}$ obtained from FTIR spectrum; (d–e) C1s and O1s region of soot; (f) Concentration of functional groups.

Notably, the YMH-Fe1 and YMH-Fe2 soot yield is reduced by 7% and 23%, respectively, compared with that of YMH soot. From the distribution pattern of the number concentration of soot particles, it can be seen that the percentage of aggregates with particle size above 1 μm increases significantly after the addition of iron. And the D_f of YMH-Fe2 soot is significantly higher than that of YMH, which indicates that the particles are more tightly agglomerated and less likely to be broken into tiny particles. Therefore, the difficulty of carbon soot replenishment is reduced. As mentioned above, although the iron content in YMH-Fe1 and YMH-Fe2 soot increases, no iron-containing soot particles are observed in the HRTEM images of soot, and the presence of crystalline iron is not found in the soot XPS spectrum. A large amount of H_2 and CO are released during coal primary pyrolysis and form a local reducing atmosphere. Fe^{3+} is converted into iron atoms or Fe^{2+} in a reducing atmosphere. The concentration of iron in the pyrolysis atmosphere is insufficiently high in this experiment; thus, the probability of the induced nucleation process of iron oxide is decreased. In the final formed soot particles, the particle size of the primary particles is significantly reduced, and the shape is more irregular, but the overall graphitization degree is higher. More amorphous cores are observed in primary soot particles, and the collision and coalescence process between nascent nanoparticles is more obvious. In addition, the aliphatic content on the surface of the soot decreases, and the C—O functional group increases, but the overall oxygen content does not increase. By analyzing the physical and chemical properties of soot, iron does not directly participate in the nucleation and surface growth of soot, but mainly promotes the oxidation reaction of soot. In line with literature [74,75] this scheme implies the transfer of oxygen chemisorbed on active Fe surface sites to the soot via physical contact points to be a crucial step. The transferred oxygen species finally stick on active soot sites to form C—O function, and their decomposition leads to the production of gaseous. Thus, the final soot yield is reduced. The increase in oxygen-containing functional groups on the soot surface indicates that it has more surface defects and active sites, which are more likely to react in the presence of oxygen combustion. The ability of iron as an additive to reduce soot during coal combustion may be more significant.

5. Conclusion

(1) The YMH-Fe1 and YMH-Fe2 soot yield is reduced by 7% and 23%, respectively, compared with that YMH soot. Iron inhibits the conversion of coal to soot, and the suppression effect intensifies with the increase in iron content.
(2) The diameter of soot primary particles is reduced from 51.1 nm to 38.7 and 39.1 nm. Iron inhibits the surface growth process of soot.
(3) The proportion of particles with particle size >1 μm due to the involvement of iron reduces the soot capture difficulty.
(4) Iron reduces the curvature of the crystallite layer and increases the graphitization of the graphite shell.
(5) In the pyrolysis process, with the participation of iron, more oxygen is involved in the generation of carbon soot, which promotes the oxidation reaction of soot. Therefore, there are more C—O functional groups on the surface of YMH-Fe soot.

Author statement

Jianmin Gao and Qian Du: Conceptualization, Methodology, Validation; Dun Li: Methodology, Formal analysis, Investigation, Data curation, Writing – original draft; Ziqi Zhao: Data curation, Visualization; Heming Dong: Methodology, Project administration; Zhaoyang Cui: Resources, Visualization.

Declaration of competing interest

The authors declare that they have no known competing financial interests or personal relationships that could have appeared to influence the work reported in this paper.

Acknowledgments

This work was supported by the National Natural Science Foundation (grant number 51676059) and National Key R&D Program of China (Grant Nos. 2018YFF0216005).

References

[1] World Coal Association, 2021. https://www.worldcoal.org/coal/uses-coal/coal-electricity (accessed on April 6, 2021).
[2] Dai SF, Finkelman RB. Coal as a promising source of critical elements: progress and future prospects. Int J Coal Geol 2018;186:155–64.
[3] Wang Y, Chung SH. Soot formation in laminar counterflow flames. Prog Energy Combust Sci 2019;74:152–238.
[4] Trubetskaya A, Jensen PA, Jensen AD, Llamas ADG, Umeki K, Gardini D, Kling J, Bates RB, Glarborg P. Effects of several types of biomass fuels on the yield, nanostructure and reactivity of soot from fast pyrolysis at high temperatures. Appl Energy 2016;171:468–82.
[5] Wu SH, Yang WM, Xu HP, Jiang Y. Investigation of soot aggregate formation and oxidation in compression ignition engines with a pseudo bi-variate soot model. Appl Energy 2019;253:12.
[6] Karatas AE, Guelder OL. Soot formation in high pressure laminar diffusion flames. Prog Energy Combust Sci 2012;38:818–45.
[7] Bond TC, Doherty SJ, Fahey DW, Forster PM, Berntsen T, DeAngelo BJ, Flanner MG, Ghan S, Kaercher B, Koch D, Kinne S, Kondo Y, Quinn PK, Sarofim MC, Schultz MG, Schulz M, Venkataraman C, Zhang H, Zhang S, Bellouin N, Guttikunda SK, Hopke PK, Jacobson MZ, Kaiser JW, Klimont Z, Lohmann U, Schwarz JP, Shindell D, Storelvmo T, Warren SG, Zender CS. Bounding the role of black carbon in the climate system: a scientific assessment. J Geophys Res Atmos 2013;118:5380–552.
[8] Wu S, Akroyd J, Mosbach S, Brownbridge G, Parry O, Page V, Yang W, Kraft M. Efficient simulation and auto-calibration of soot particle processes in Diesel engines. Appl Energy 2020:262.
[9] Pang KM, Karvounis N, Walther JH, Schramm J. Numerical investigation of soot formation and oxidation processes under large two-stroke marine diesel engine-like conditions using integrated CFD-chemical kinetics. Appl Energy 2016;169:874–87.
[10] Kruse S, Ye JJ, Sun ZW, Attili A, Dally B, Medwell P, Pitsch H. Experimental investigation of soot evolution in a turbulent non-premixed prevaporized toluene flame. Proc Combust Inst 2019;37:849–57.
[11] Soussi JP, Demarco R, Consalvi JL, Liu F, Fuentes A. Influence of soot aging on soot production for laminar propane diffusion flames. Fuel 2017;210:472–81.
[12] Vargas AM, Gulder OL. Pressure dependence of primary soot particle size determined using thermophoretic sampling in laminar methane-air diffusion flames. Proc Combust Inst 2017;36:975–84.
[13] Schulz F, Commodo M, Kaiser K, De Falco G, Minutolo P, Meyer G, D'Anna A, Gross L. Insights into incipient soot formation by atomic force microscopy. Proc Combust Inst 2019;37:885–92.
[14] Dreyer JAH, Poli M, Eaves NA, Botero ML, Akroyd J, Mosbach S, Kraft M. Evolution of the soot particle size distribution along the centreline of an n-heptane/toluene co-flow diffusion flame. Combust Flame 2019;209:256–66.
[15] Luo MY, Liu D. Effects of dimethyl ether addition on soot formation, evolution and characteristics in flame-wall interactions. Energy 2018;164:642–54.
[16] Liu Y, Cheng XB, Qin LJ, Wang X, Yao JJ, Wu H. Experimental investigation on soot formation characteristics of n-heptane/butanol isomers blends in laminar diffusion flames. Energy 2020;211:13.
[17] Apicella B, Russo C, Cerciello F, Stanzione F, Ciajolo A, Scherer V, Senneca O. Insights on the role of primary and secondary tar reactions in soot inception during fast pyrolysis of coal. Fuel 2020:275.
[18] Chang Q, Gao R, Li H, Yu G, Wang F. Effect of CO2 on the characteristics of soot derived from coal rapid pyrolysis. Combust Flame 2018;197:328–39.
[19] Centrone A, Brambilla L, Renouard T, Gherghel L, Mathis C, Mullen K, Zerbi G. Structure of new carbonaceous materials: the role of vibrational spectroscopy. Carbon 2005;43:1593–609.
[20] Fletcher TH, Ma JL, Rigby JR, Brown AL, Webb BW. Soot in coal combustion systems. Prog Energy Combust Sci 1997;23:283–301.
[21] Gai ZK, Zhang R, Bi JC. Characteristics of soot from rapid pyrolysis of coal and petroleum coke. Energy Fuels 2017;31:3759–67.
[22] Kazakov A, Wang H, Frenklach M. Detailed modeling OF soot formation IN laminar premixed ethylene flames at a pressure OF 10 bar. Combust Flame 1995;100:111–20.
[23] Frenklach M. Reaction mechanism of soot formation in flames. Phys Chem Chem Phys 2002;4:2028–37.
[24] Thomson M, Mitra T. A radical approach to soot formation. Science 2018;361:978–9.
[25] Johansson KO, Head-Gordon MP, Schrader PE, Wilson KR, Michelsen HA. Resonance-stabilized hydrocarbon-radical chain reactions may explain soot inception and growth. Science 2018;361:997–1000.
[26] Zhang H. Nitrogen evolution and soot formation during secondary coal pyrolysis, Chemical Engineering. Provo: Brigham Young University; 2001.
[27] Nenniger RD. Aerosols produced from coal pyrolysis[D]. Massachusetts Institute of Technology, Department of Chemical Engineering; 1986.
[28] Wornat MJ, Sarofim AF, Longwell JP. Pyrolysis-induced changes in the ring number composition of polycyclic aromatic compounds from a high volatile bituminous coal[J]. Sympos Combust 1989;22(1):135–43.
[29] Zeng D, Hu S, Sayre AN, Sarv H. On the rank-dependence of coal tar secondary reactions. Proc Combust Inst 2011;33:1707–14.
[30] JL Ma, T.H. Fletcher, B.W. Webb, Effect of flame environment on soot formation in coal combustion, in: J.A. Pajares, J.M.D. Tascon (Eds.) Coal Sci, Vols I and Ii1995, pp. 869-872.
[31] Ma JL, Fletcher TH, Webb BW. Thermophoretic sampling OF coal-derived soot particles during devolatilization. Energy Fuels 1995;9:802–8.
[32] Chang QH, Gao R, Gao M, Yu GS, Mathews JP, Wang FC. Experimental analysis of the evolution of soot structure during CO2 gasification. Fuel 2020;265:11.
[33] Deng C, Liaw SB, Gao X, Wu H. Differences in soot produced from rapid pyrolysis of xylan, cellulose and lignin under pulverized-fuel conditions. Fuel 2020:265.
[34] Wang X, Li S, Adeosun A, Li Y, Vujanovic M, Tan H, Duic N. Effect of potassium-doping and oxygen concentration on soot oxidation in O-2/CO2 atmosphere: a kinetics study by thermogravimetric analysis. Energy Convers Manag 2017;149:686–97.
[35] Trubetskaya A, Larsen FH, Shchukarev A, Stahl K, Umeki K. Potassium and soot interaction in fast biomass pyrolysis at high temperatures. Fuel 2018;225:89–94.
[36] He Q, Guo Q, Umeki K, Ding L, Wang F, Yu G. Soot formation during biomass gasification: a critical review. Renew Sustain Energy Rev 2021;139.
[37] Hu C, Li W, Lin Q, Cheng X, Huang Q, Zhang H, Wang Z. Effects of ferrocene on flame temperature, formation of soot particles and growth of polycyclic aromatic hydrocarbons. J Energy Inst 2017;90:893–901.
[38] Simonsson J, Olofsson N-E, Bladh H, Sanati M, Bengtsson P-E. Influence of potassium and iron chloride on the early stages of soot formation studied using imaging LII/ELS and TEM techniques. Proc Combust Inst 2017;36:853–60.
[39] Charalampopoulos TT, Hahn DW, Chang H. Role OF metal additives IN light-scattering from flame particulates. Appl Opt 1992;31:6519–28.
[40] Feitelberg AS, Longwell JP, Sarofim AF. Metal enhanced soot and PAH formation. Combust Flame 1993;92:241–53.
[41] Agafonov GL, Smirnov VN, Vlasov PA. Effect OF iron penta-carbonyl ON soot formation behind SHOCK waves. Combust Sci Technol 2012;184:1838–61.
[42] Howard JB, Kausch WJ. Soot control by fuel additives. Prog Energy Combust Sci 1980;6:263–76.
[43] Kim SH, Fletcher RA, Zachariah MR. Understanding the difference in oxidative properties between flame and diesel soot nanoparticles: the role of metals. Environ Sci Technol 2005;39:4021–6.
[44] Wagloehner S, Baer JN, Kureti S. Structure-activity relation of iron oxide catalysts in soot oxidation. Appl Catal B Environ 2014;147:1000–8.
[45] Wagloehner S, Kureti S. Study on the mechanism of the oxidation of soot on Fe2O3 catalyst. Appl Catal B Environ 2012;125:158–65.
[46] Kim K, Hahn DW. Interaction between iron based compound and soot particles in diffusion flame. Energy 2016;116:933–41.
[47] Kim KB, Masiello KA, Hahn DW. Reduction of soot emissions by iron penta-carbonyl in isooctane diffusion flames. Combust Flame 2008;154:164–80.
[48] Braun A, Huggins FE, Kelly KE, Mun BS, Ehrlich SN, Huffman GP. Impact of ferrocene on the structure of diesel exhaust soot as probed with wide-angle X-ray scattering and C(1s) NEXAFS spectroscopy. Carbon 2006;44:2904–11.
[49] Dong H, Zhang Y, Du Q, Li D, Feng D, Gao J, Wu S. Effect of different forms of Na and temperature on soot formation during lignite pyrolysis. Fuel 2020:280.
[50] Li D, Zhang Y, Dong H, Du Q, Gao J, Cui Z. Effects of iron on the soot formation during coal pyrolysis. Fuel 2020:270.
[51] Dong H-M, Du Q, Li D, Cui Z-Y, Gao J-M, Wu S-H. Impacts of organic structures and inherent minerals of coal on soot formation during pyrolysis. Energies 2019;12.
[52] Rojas-Valencia N, Gallego J, Santamaría A. Effect of an iron compound added to diesel fuels in both soot reduction capacity and soot oxidation reactivity. Energy Fuel 2017;31:12455–65.
[53] Ma Y, Zhu M, Zhang D. The effect of a homogeneous combustion catalyst on exhaust emissions from a single cylinder diesel engine. Appl Energy 2013;102:556–62.
[54] Zhang D, Ma Y, Zhu M. Nanostructure and oxidative properties of soot from a

compression ignition engine: the effect of a homogeneous combustion catalyst. Proc Combust Inst 2013;34:1869–76.
[55] Wang Y-f, Huang Q-x, Wang F, Chi Y, Yan J-h. Brownian dynamics simulation of soot primary particle aggregation in laminar ethylene diffusion flames. Phys Stat Mech Appl 2019;514:936–47.
[56] Brasil AM, Farias TL, Carvalho MG. A recipe for image characterization of fractal-like aggregates. J Aerosol Sci 1999;30:1379–89.
[57] Soriano JA, Agudelo JR, Lopez AF, Armas O. Oxidation reactivity and nanostructural characterization of the soot coming from farnesane - a novel diesel fuel derived from sugar cane. Carbon 2017;125:516–29.
[58] Gaddam CK, Vander Wal RL. Physical and chemical characterization of SIDI engine particulates. Combust Flame 2013;160:2517–28.
[59] Cadrazco M, Santamaria A, Agudelo JR. Chemical and nano-structural characteristics of the particulate matter produced by renewable diesel fuel in an automotive diesel engine. Combust Flame 2019;203:130–42.
[60] Tang Q, Wang M, You X. Effects of fuel structure on structural characteristics of soot aggregates. Combust Flame 2019;199:301–8.
[61] Yehliu K, Vander Wal RL, AL Boehman. Development of an HRTEM image analysis method to quantify carbon nanostructure. Combust Flame 2011;158:1837–51.
[62] Wang Ca, Huddle T, Huang C-H, Zhu W, Vander Wal RL, Lester EH, Mathews JP. Improved quantification of curvature in high-resolution transmission electron microscopy lattice fringe micrographs of soots. Carbon 2017;117:174–81.
[63] Liu J, Wang L, Sun P, Wang P, Li Y, Ma H, Wu P, Liu Z. Effects of iron-based fuel borne catalyst addition on microstructure, element composition and oxidation activity of diesel exhaust particles. Fuel 2020;270:117597.
[64] Raj A, Tan Z, Zhu D, Croiset E, Wen JZ. On the particle evolution in iron pentacarbonyl loaded counterflow methane–air flame. Combust Flame 2018;194:1–14.
[65] Zickler GA, Smarsly B, Gierlinger N, Peterlik H, Paris O. A reconsideration of the relationship between the crystallite size L-a of carbons determined by X-ray diffraction and Raman spectroscopy. Carbon 2006;44:3239–46.
[66] Ivleva NP, Messerer A, Yang X, Niessner R, Poeschl U. Raman microspectroscopic analysis of changes in the chemical structure and reactivity of soot in a diesel exhaust aftertreatment model system. Environ Sci Technol 2007;41:3702–7.
[67] Russo C, Ciajolo A. Effect of the flame environment on soot nanostructure inferred by Raman spectroscopy at different excitation wavelengths. Combust Flame 2015;162:2431–41.
[68] Larouche N, Stansfield BL. Classifying nanostructured carbons using graphitic indices derived from Raman spectra. Carbon 2010;48:620–9.
[69] Al-Qurashi K, Boehman AL. Impact of exhaust gas recirculation (EGR) on the oxidative reactivity of diesel engine soot. Combust Flame 2008;155:675–95.
[70] Knauer M, Carrara M, Rothe D, Niessner R, Ivleva NP. Changes in structure and reactivity of soot during oxidation and gasification by oxygen, studied by micro-Raman spectroscopy and temperature programmed oxidation. Aerosol Sci Technol 2009;43:1–8.
[71] Marhaba I, Ferry D, Laffon C, Regier TZ, Ouf F-X, Parent P. Aircraft and Mini-CAST soot at the nanoscale. Combust Flame 2019;204:278–89.
[72] Feng DD, Guo DW, Zhang Y, Sun SZ, Zhao YJ, Shang Q, Sun HL, Wu JQ, Tan HP. Functionalized construction of biochar with hierarchical pore structures and surface O-/N-containing groups for phenol adsorption. Chem Eng J 2021;410.
[73] Feng DD, Shang Q, Dong HM, Zhang Y, Wang ZL, Li D, Xie M, Wei QY, Zhao YJ, Sun SZ. Catalytic mechanism of Na on coal pyrolysis-derived carbon black formation: experiment and DFT simulation. Fuel Process Technol 2021:224.
[74] Mul G, Kapteijn F, Doornkamp C, Moulijn JA. Transition metal oxide catalyzed carbon black oxidation: a study with18O2. J Catal 1998;179:258–66.
[75] Reichert D, Bockhorn H, Kureti S. Study of the reaction of NOx and soot on Fe2O3 catalyst in excess of O2. Appl Catal B Environ 2008;80:248–59.